COMMUNICATIONS IN SCIENCE AND TECHNOLOGY
Homepage: cst.kipmi.or.id

Block-based optimization for enhancing reversible watermarking using reduced difference expansion

Aulia Arham[a], Hanung Adi Nugroho[b*]

[a]*Department of Information Systems, Universitas Negeri Islam Imam Bonjol, Padang 25171, Indonesia*
[b]*Department of Electrical and Information Engineering, Universitas Gadjah Mada, Yogyakarta 55281, Indonesia*

Article history:
Received: 3 January 2024 / Received in revised form: 17 May 2024 / Accepted: 4 June 2024

Abstract

In recent years, reversible watermarking has emerged as a promising technique that safely embeds data in digital images without compromising their originality. This method is particularly useful for sensitive images such as military, art, and medical images, where each pixel contains important information requiring authentication. Researchers have been attempting to develop this method further to increase payload capacity while maintaining visual quality and low computational complexity. In this study, we developed a reversible watermarking with block-based optimization based on Reduced Difference Expansion (RDE) applied to 3×3 pixel blocks, allowing for the embedding of $8-$bit data. Based on experimental results from tests conducted on 2 common images and 3 medical images, our method could consistently achieve a payload capacity of up to 0.8924 bpp with a PSNR of 41.077 dB while maintaining good visual quality across various image categories, outperforming previous approaches.

Keywords: Reversible watermarking; digital images; reduced difference expansion.

1. Introduction

In the digital information era, preserving data integrity while ensuring security remains a critical concern [1]–[4], particularly in the realm of image processing. Reversible watermarking techniques offer a promising solution, allowing for the secure integration of additional data into digital images without compromising the original content. Implementing such techniques becomes crucial, particularly in handling sensitive imagery such as military, artwork, and medical images, where every pixel encapsulates crucial information requiring authentication [5]–[9]. One such method, Difference Expansion (DE), has shown potential in reversible data embedding due to its ability to embed information while maintaining reversibility [10]–[12].

Tian [13], [14] introduced the Difference Expansion (DE) technique, representing a clear example of reversible watermarking. The DE method operates by concealing data within the discrepancies among pixel pairs. These differences are broken down into an eight-bit field, and the data bits are embedded into the least significant bit, resulting in an increase in the value of the differences between pairs of pixels. Recent years have witnessed rapid advancements in various reversible watermarking approaches, most of which are from the foundational DE method. These advancements concentrate on enhancing DE method performance parameters, including payload capacity, visual quality, and computational complexity.

Multiple techniques have been introduced by researchers to improve the visual quality of the image. Liu et al. [15], for example, introduced reduced difference expansion (RDE), while Yi et al. [16] developed enhanced reduced difference expansion (IRDE), both of which successfully improved visual quality of the image. In contrast, Abdullah and Manaf [17] proposed embedding data in the smooth areas of the image using the DE method, and Maniriho and Ahmad [18] suggested using the DE method combined with the modulus function in those areas, also contributing to improved image quality despite reducing payload capacity. To increase capacity, researchers have explored block size variations. Alattar introduced methods [19] and [20] using blocks of 1×3 and 2×2 pixels as a basis. Hsiao et al. [21] utilized 3×3 blocks. Ahmad et al. [22] used 2×2 blocks while reducing the difference value with the RDE method. Arham et al. [10]–[12] and Al Huti et al. [23] used 2×2 and 4×4 blocks, respectively, by modifying the RDE method. In addition, Syahlan and Ahmad [24] applied 2×2 blocks and changed

*Corresponding Author.
Email: adinugroho@ugm.ac.id
https://doi.org10.21924/cst.9.1.2024.1368

the pixel difference values with modified RDE. These strategies extended data embedding and yielded favorable visual quality. Other researchers have combined various algorithms based on DE to enhance the embedding capacity and visual quality in digital images. For instance, Dragoi and Coltuc [25] proposed the utilization of local predictions in extending reversible difference watermarking. Some studies, such as [26]–[29], have proposed a combination of interpolation and DE, while other researchers, like those mentioned in [18], [30]–[32], have suggested a combination of the DE method and the modulus function. Additionally, some researchers combined the DE method with error-based prediction, as shown in studies [33]–[35]. The combination of the DE method and histogram shifting has also been applied by the researchers in [36], [37]. Mehbodniya et al. [38] proposed a multilevel thresholding method to reduce the difference value in pixels. Arham and Lestari [11] proposed a novel approach by combining the DE method with Arnold's cat map.

In reversible watermarking, there are two pivotal factors that necessitate improvement: the resemblance between the original cover image and the resultant watermark-image, and the payload capacity for the embedded data [12]. Enhancing the resemblance between the cover and watermark images is essential to ensure that any alterations caused by embedding remain imperceptible for human eye. Simultaneously, augmenting the payload capacity of embedded data is crucial for accommodating more information without significantly impacting the image quality. Balancing these factors is the key to achieve the efficient reversible watermarking methods with increased data-hiding capacity while preserving visual fidelity. This paper presents an exploration into the optimization of reversible data embedding through a block-based approach using the RDE technique. By leveraging pixel blocks and refining the RDE method, this research aims to enhance the performance and technical capabilities of existing reversible watermarking methods. The study focuses on improving the method's efficiency in embedding data while preserving the visual quality of images, aiming to significantly contribute to the field of secure data embedding in digital images.

The paper is organized into four sections. The initial section introduces the fundamental research context and reviews previous studies related to the difference expansion method. Section 2 provides a detailed explanation of our proposed method, including the data-embedding method and data-extraction method. Section 3 meanwhile presents the experimental results and compares them with the previous method, focusing on payload capacity, visual quality, and computational complexity. Finally, Section 4 presents a summary of the findings in the study.

2. Materials and Method

The proposed method aims to increase reversible watermarking technique through pixel block usage and minimize the expansion of differences between pixel pairs. This method was designed to improve the technical capabilities of previous research, especially the methods [23] and [24]. The significant contribution of this research is to improve the performance of reversible watermarking in images by optimizing the block size used and improving the reduce difference expansion method. In the pursuit of enhancing block optimization, this proposed method adopted 3×3 blocks that can embed 8 bits, as depicted in Fig. 1(c), diverging from prior approaches such as Al Huti et al. [23] 4×4 blocks that could embed 15 bits as illustrated in Fig. 1(a) and Syahlan and Ahmad [24] that used 2×2 blocks that could embed 3 bits, as depicted in Fig. 1(b). Tabel 1 presents the reduction schemes exemplified by Al Huti et al. [23] in Equation (2), Syahlan and Ahmad [24] in Equation (3), and the proposed method in Equation (4) with the corresponding outcomes detailed in Table 2. Employing the approach outlined in (4), the difference values after data embedding using our method closely aligned with the original values, displaying a closer proximity compared to those obtained through (2) and (3).

2.1. Data-Embedding Method

The following describes the four key stages of the embedding process:

Step 1: The image is partitioned into 3×3 blocks. A pixel vector subsequently is formulated for each block to calculate the disparities between consecutive pixels, depicted in Fig. 1(c). The pixel x_4 is established as the reference point, as shown in Fig. 1. This reference facilitates the derivation of vectors $h = (h_0, h_1, h_2, h_3, h_4, h_5, h_6, h_7, h_8)$, representing the differences within the vector $x = (x_0, x_1, x_2, x_3, x_4, x_5, x_6, x, x_8)$, and can be articulated in equation (1).

$$\begin{cases} h_0 = x_0 - x_4 \\ h_1 = x_1 - x_4 \\ \quad \vdots \quad \vdots \quad \vdots \\ h_4 = 0 \\ h_5 = x_5 - x_4 \\ \quad \vdots \quad \vdots \quad \vdots \\ h_8 = x_8 - x_4 \end{cases} \tag{1}$$

Step 2: Following the computation of pixel block pair differences to mitigate distortion in the values, Equation (4) is utilized, wherein h is determined using Equation (5). The process of reducing the difference value is conducted based on the condition $(-1 > h_i > 1)$, where the Location Map $(EM_{h_i}) = (0,1)$ is set to $(0,1)$. Conversely, if $(-1 \leq h_i \leq 1)$, the Location Map $(EM_{h_i}) = (-1)$ is set to (-1) as demonstrated in (6). During the extraction phase, the Location Map (EM) is instrumental in restoring the initial pixels value from the original image.

$$h_i' = \begin{cases} h_i - \left(2^{\lfloor \log_2(h_i) \rfloor} + \lfloor \log_2(h_i) \rfloor\right), & \text{if } h_i > 1 \\ h_i + \left(2^{\lfloor \log_2(h_i) \rfloor} + \lfloor \log_2(h_i) \rfloor\right), & \text{if } h_i < -1 \end{cases} \tag{2}$$

$$h_i' = \begin{cases} h_i - \left(2^{\lfloor \log_2(h_i) \rfloor} + (2 + \lfloor \log_2(h_i) \rfloor)\right), & \text{if } h_i > 1 \\ h_i + \left(2^{\lfloor \log_2(h_i) \rfloor} + (2 + \lfloor \log_2(h_i) \rfloor)\right), & \text{if } h_i < -1 \end{cases} \tag{3}$$

$$h_i' = \begin{cases} h_i - 2^{\lfloor \log_2(h_i) \rfloor - 1}, & \text{if } 2 \times 2^{l-1} \leq d_i \leq 3 \times 2^{l-1} - 1 \\ h_i - 2^{\log_2(h_i)}, & \text{if } 3 \times 2^{l-1} \leq d_i \leq 4 \times 2^{l-1} - 1 \end{cases} \tag{4}$$

$$l = \lfloor \log_2 |h_i| \rfloor \tag{5}$$

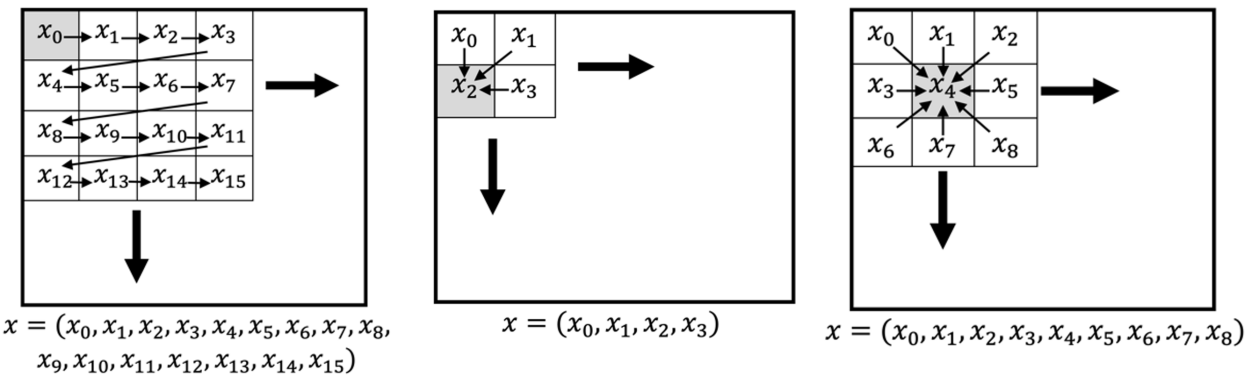

(a) (b) (c)

Fig. 1. The differences of use block (a) the method of [23] (b) the method of [24] (c) the proposed method

Table 1. Comparison in the calculation of the reduced difference expansion

h_i	h'_i		
	Al Huti et al. [23]	Syahlan and Ahmad [24]	Our method
$h_0 = 60$	$60-(2^{\lfloor \log_2(60) \rfloor}+\lfloor \log_2(60) \rfloor)=23$	$60-(2^{\lfloor \log_2(60) \rfloor}+(2+\lfloor \log_2(60) \rfloor))=21$	$60-2^{\lfloor \log_2(60) \rfloor}=28$
$h_1 = 45$	$45-(2^{\lfloor \log_2(45) \rfloor}+\lfloor \log_2(45) \rfloor)=8$	$45-(2^{\lfloor \log_2(45) \rfloor}+(2+\lfloor \log_2(45) \rfloor))=6$	$45-2^{\lfloor \log_2(45) \rfloor}=29$
$h_2 = 25$	$25-(2^{\lfloor \log_2(25) \rfloor}+\lfloor \log_2(25) \rfloor)=5$	$25-(2^{\lfloor \log_2(25) \rfloor}+(2+\lfloor \log_2(25) \rfloor))=9$	$25-2^{\lfloor \log_2(25) \rfloor}=3$

Table 2. Camparison of the value difference after reduction

h_i	$b_i = 0 \longrightarrow h_i-(2\times h'_i+0)$			$b_i = 0 \longrightarrow h_i-(2\times h'_i+1)$		
	Al Huti et al. [23]	Syahlan and Ahmad [24]	Our method	Al Huti et al. [23]	Syahlan and Ahmad [24]	Our method
$h_0 = 60$	$60-46=14$	$60-42=18$	$60-56=4$	$60-47=15$	$60-43=19$	$60-57=3$
$h_0 = 45$	$45-16=29$	$45-12=33$	$45-58=-13$	$45-17=28$	$45-13=32$	$45-59=-14$
$h_0 = 25$	$25-10=15$	$25-6=19$	$25-18=7$	$25-11=16$	$25-7=18$	$25-19=6$

$$EM_{h_i} = \begin{cases} -1, \text{ if } -1 > h_i > 1 \\ 0, \text{ if } 2\times 2^{l-1} \le h_i \le 3\times 2^{l-1}-1 \\ 1, \text{ if } 3\times 2^{l-1} \le h_i \le 4\times 2^{l-1}-1 \end{cases} \quad (6)$$

Step 3: To embed a data bit b_i, there are two available methods: (7) or (8). The blocks of pixels using Equation (7) for data embedding are classified as expandable, denoted by Location Map $(EM_b) = 1$. In cases where Equation (7) leads to underflow or overflow, the reduction of the difference value is ceased, and the embedding process shifts to (8), labeled as changeable with Location Map $(EM_b) = 0$. Furthermore, blocks not fitting into the second category, where embedding data is not executed, are classified as unchangeable with Location Map $(EM_b) = -1$.

$$\begin{cases} \tilde{h}_0 = 2\times h'_0 + b_i \\ \tilde{h}_1 = 2\times h'_1 + b_{i+1} \\ \vdots \quad \vdots \quad \vdots \\ \tilde{h}_4 = 0 \\ \tilde{h}_5 = 2\times h'_5 + b_{i+4} \\ \vdots \quad \vdots \quad \vdots \\ \tilde{h}_8 = 2\times h'_8 + b_{i+7} \end{cases} \quad (7)$$

$$\begin{cases} h'_0 = 2\times \left\lfloor \frac{h_0}{2} \right\rfloor + b_i \\ h'_1 = 2\times \left\lfloor \frac{h_1}{2} \right\rfloor + b_{i+1} \\ \vdots \quad \vdots \quad \vdots \\ h'_1 = 0 \\ h'_5 = 2\times \left\lfloor \frac{h_5}{2} \right\rfloor + b_{i+4} \\ \vdots \quad \vdots \quad \vdots \\ h'_8 = 2\times \left\lfloor \frac{h_8}{2} \right\rfloor + b_{i+7} \end{cases} \quad (8)$$

Step 4: Each block of pixels is associated with an embedding location map, $EM = (EM_1, EM_2, EM_3, EM_4, EM_5, EM_6, EM_7, EM_8, EM_9)$, where EM_1 classifies the block pixel categories into expandable, changeable, or non-changeable regarding EM_b. EM_2, EM_3, EM_4, EM_5, EM_6, EM_7, EM_8, and EM_9 are linked to EM_{h_i}, identifying the reduced difference values of the pixel $h = (h_0, h_1, h_2, h_3, h_5, h_6, h_7, h_8)$ within the block. In cases where Location Map $(EM_1) = 0$, EM_2, EM_3, EM_4, EM_5, EM_6, EM_7, EM_8,and EM_9 are set to 1 if the difference value of pixel $h = (h_0, h_1, h_2, h_3, h_5, h_6, h_7, h_8)$ is odd. Conversely, if the difference value of pixel $h = (h_0, h_1, h_2, h_3, h_5, h_6, h_7, d_8)$ is even, then EM_2, EM_3, EM_4, EM_5, EM_6, EM_7, EM_8,and EM_9 are set to 0. After finalizing the embedding process, the subsequent

step entails generating a new pixel x_i' according to equation (9).

$$\begin{cases} x_0' = \tilde{h}_0 + x_4 \\ x_1' = \tilde{h}_1 + x_4 \\ \quad \vdots \quad \vdots \quad \vdots \\ x_4' = x_4 \\ x_5' = \tilde{h}_5 + x_4 \\ \quad \vdots \quad \vdots \quad \vdots \\ x_8' = \tilde{h}_8 + x_4 \end{cases} \tag{9}$$

2.2. Data-Extracting Method

The extraction process involves retrieving the concealed data and reconstructing the original image, executed as follows:

Step 1: The watermark image is partitioned into 3×3 pixel blocks, converted into the vector x', and then the differences between pixel block pairs, denoted as x', are calculated using Equation (1).

Step 2: Employing the location map EM, the concealed data within the least significant bit (LSB) differences $\tilde{h}$ is revealed, excluding instances where the value of EM_b is -1. If the location map EM_b is 1, the restoration of the original image appearance is achieved using the location map EM_{h_i} through Equation (10), while Equation (11) is utilized when the location map EM_b is 0.

$$h_i = \begin{cases} h_i' + 2^{\log_2 |h_i'|+1}, & \text{if } EM_{h_i} = 1 \\ h_i' + 2^{\log_2 |h_i'|}, & \text{if } EM_{h_i} = 0 \end{cases} \tag{10}$$

$$h_i = \begin{cases} 2 \times \left\lfloor \frac{h_i'}{2} \right\rfloor + 1, & \text{if } EM_{h_i} = 1 \\ 2 \times \left\lfloor \frac{h_i'}{2} \right\rfloor, & \text{if } EM_{h_i} = 0 \end{cases} \tag{11}$$

Step 3: To reconstruct the original image, the following Equation (12) is applied:

$$\begin{cases} x_0 = h_0 + x_4 \\ x_1 = h_1 + x_4 \\ \quad \vdots \quad \vdots \quad \vdots \\ x_4 = x_4 \\ x_5 = h_5 + x_4 \\ \quad \vdots \quad \vdots \quad \vdots \\ x_8 = h_8 + x_4 \end{cases} \tag{12}$$

3. Results and Discussion

In this experiment, a thorough assessment was carried out to compare the method performance, the payload capacity of the image, and the visual quality after the embedding process of the proposed technique with the existing methods outlined in references [23] and [24]. We conducted comprehensive simulations using five types of grayscale images, comprising two common images (Baboon and Peppers) and three medical images (Head, Leg, and X-ray), each of which had the dimensions of 512×512 pixels, as shown in Fig. 2.

3.1. Performance

The experiments conducted showed the effective functioning of both the embedding and extraction processes. These processes demonstrated an ability to restore an image to its original state. Fig. 3 demonstrates the original image after data embedding, showcasing the watermark image obtained from the process. Notably, the visual quality of the cover image is well-preserved. In Figs. 3(a) to 3(e) and 3(f) to 3(j), displaying the original and watermark images, respectively, the similarity is strikingly high among the five sets, making it relatively challenging to discern differences between the original and watermark images. These observations underlined the exceptional quality of the watermark images, maintaining a high degree of similarity with the original images. The computational time required for processing different images (Baboon, Peppers, Head, Leg, and X-Ray) was measured in seconds, as shown in Table (3). In the case of the common Baboon image, the proposed method exhibited a longer computational time of 96.45 seconds, compared to Al Huti et al. [23] at 47.86 seconds and Syahlan and Ahmad [24] at 23.06 seconds. For the Peppers image, the proposed method showed a higher computational time of 91.23 seconds, surpassing Al Huti et al. [23] at 46.74 seconds and Syahlan and Ahmad [24] at 23.15 seconds. Regarding the Head medical image, the proposed method indicated a computational time of 90.12 seconds, slightly higher than that of Al Huti et al. [23] at 45.71 seconds and Syahlan and Ahmad [24] at 23.54 seconds. Across the Leg and X-Ray medical images, the proposed method consistently displayed higher computational times compared to Al Huti et al. [23] and Syahlan and Ahmad [24]. The Leg image reports a computational time of 93.97 seconds, while the X-Ray image showed a time of 89.44 seconds using the proposed method.

Although the proposed method exhibited higher computational times, this aspect signified more intricate operations or computations required to accomplish specific objectives. Unlike the method of Al Huti et al. [23] and Syahlan and Ahmad [24] where reduction was limited to expandable categorized our method executed the reduction in pixel pair values across all blocks. This comprehensive approach contributes to the extended computational time required by our method compared to the others.

3.2. Payload capacity

The payload capacity of embedding data refers to the amount of bit data that can be embedded into the image, This capacity is measured in bits per pixel (bpp). Table 3 shows the analysis in the data capacities in bits across several image types, including widely used images like Baboon and Peppers, along with medical images such as Head, Leg, and X-Ray. These capacities were compared among three distinct methods: Al Huti et al. [23], Syahlan and Ahmad [24], and the proposed method. For the common image Baboon, the proposed method demonstrated a data capacity of $233,928$ bits (0.89 bpp), slightly lower than that of Al Huti et al. [23] $245,760$ bits (0.94 bpp) but notably higher than Syahlan and Ahmad [24] $196,608$ bits (0.75 bpp). In the case of the Peppers image, the proposed method showcased a similar capacity of $233,928$ bits (0.89 bpp), almost matching Al Huti et al. [23] $245,595$ bits (0.94 bpp) and significantly surpassing Syahlan and Ahmad [24] $196,593$ bits (0.75 bpp).

Examining the Head medical image, the proposed method presented a higher capacity of $228,376$ bits (0.87 bpp), outperforming Syahlan and Ahmad [24] $191,652$ bits (0.73 bpp), al-

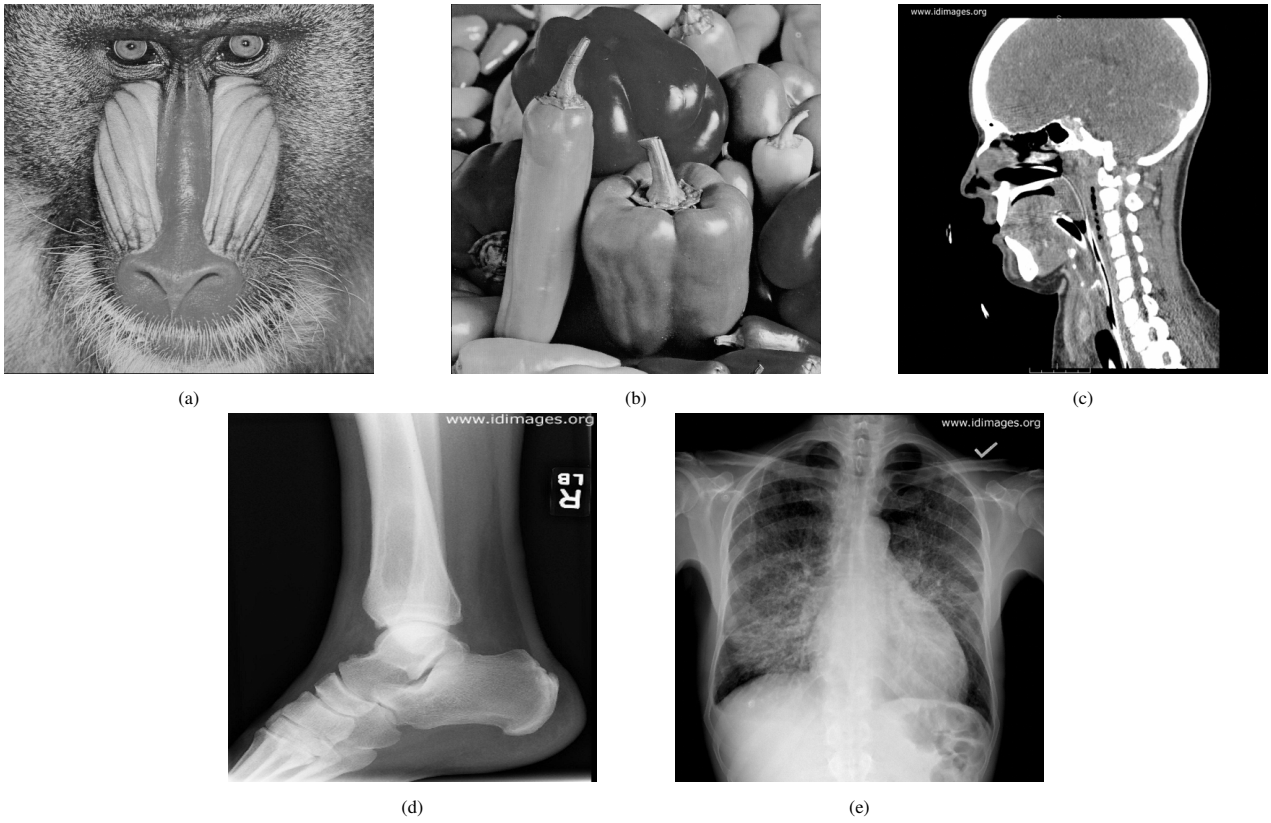

Fig. 2. The two common images and three medical images used for testing are: (a) Baboon, (b) Peppers, (c) Head, (d) Leg, and (e) X-Ray.

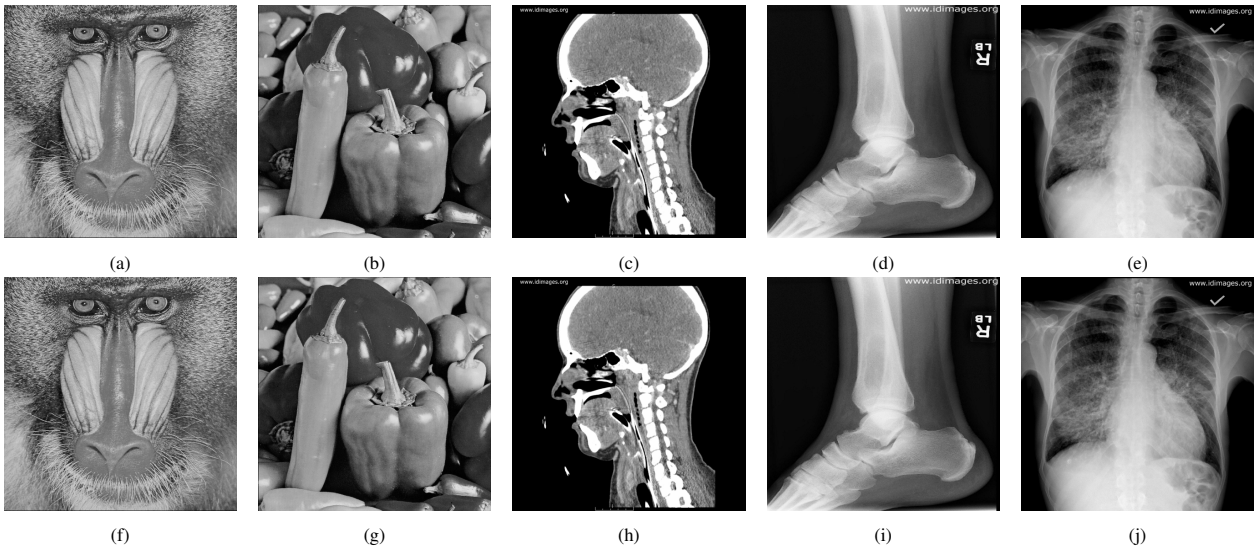

Fig. 3. An example of embedding images (a) Baboon after embedding (b) Peppers after embedding (c) Head after embedding (d) Leg after embedding (e) X-Ray after embedding (f) Baboon after extraction (g) Peppers after extraction (h) Head after extraction (i) Leg after extraction (f) X-Ray after extraction

though it was slightly lower than Al Huti et al. [23] 221,625 bits (0.85 bpp). Regarding the Leg and X-Ray medical images, the proposed method displayed competitive capacities compared to Al Huti et al. [23] and Syahlan and Ahmad [24]. The Leg image demonstrated a capacity of 233,704 bits (0.89 bpp) with the proposed method, while the X-Ray image showcased a capacity of 233,904 bits (0.89 bpp).

Overall, the proposed method consistently presented competitive or slightly lower capacities compared to Al Huti et al. [23], while outperforming or closely aligning with the capacities achieved by Syahlan and Ahmad [24] across diverse image categories. This highlights the reliability and efficacy of the proposed method in embedding data across various image types.

3.3. Visual quality

After embedding data into the images using the proposed technique, an extensive analysis of the visual quality was conducted. The assessment primarily focused on evaluating the visual fidelity and perceptibility of the images. This involved examining the alterations or distortions in the images post-

Table 3. Comparing the capacity of embedding data

Images	Capacity (bits)			Embedding capacity (bpp)			Computational Time (Second)		
	Al Huti et al. [23]	Syahlan & Ahmad [24]	Our method	Al Huti et al. [23]	Syahlan & Ahmad [24]	Our method	Al Huti et al. [23]	Syahlan & Ahmad [24]	Our method
Baboon	245,760	196,608	233,928	0.93750	0.75000	0.89236	47.86	23.06	96.45
Peppers	245,595	196,593	233,928	0.93687	0.74994	0.89236	46.74	23.15	91.23
Head	221,625	191,652	228,376	0.84543	0.73109	0.87119	45.71	23.54	90.12
Leg	241,905	195,720	233,704	0.92279	0.74661	0.89151	45.76	23.02	93.97
X-Ray	238,320	195,435	233,904	0.90912	0.74553	0.89227	63.52	41.97	89.44

Table 4. Comparing the quality of watermarking images using PSNR

Images	Embedding capacity (bpp)			PSNR (dB)		
	Al Huti et al. [23]	Syahlan and Ahmad [24]	Our method	Al Huti et al. [23]	Syahlan and Ahmad [24]	Our method
Baboon	0.93750	0.75000	0.89236	23.904	22.963	33.586
Peppers	0.93687	0.74994	0.89236	29.730	28.241	40.507
Head	0.84543	0.73109	0.87119	31.028	29.729	40.404
Leg	0.92279	0.74661	0.89151	34.977	33.163	44.201
X-Ray	0.90912	0.74553	0.89227	32.985	31.952	44.196

embedding compared to their original versions. The aim was to ensure that the embedded data did not significantly compromise the visual quality or introduce noticeable distortions that could impact the overall appearance or interpretability of the images. Peak Signal-to-Noise Ratio (PSNR) was employed in this study to measure and compare the cover image quality before and after the embedding data, calculated through Equation (13).

$$PSNR = 10\log_{10}\frac{255^2}{\frac{1}{m\times n}\sum_{i}^{m-1}\sum_{j}^{n-1}|I(i,j)-I'(i,j)|^2} \quad (13)$$

The analysis based on Table 4 shows the visual quality at maximum payload across several image types. According to Table 4, our proposed method consistently exhibits higher PSNR values than the other methods. Based on the provided PSNR (Peak Signal-to-Noise Ratio) data across different bpp (bits per pixel) settings for various images, as shown in Fig. 4, here are the comparative discussions for the Baboon image, when comparing Al Huti et al., Syahlan and Ahmad, and our proposed method, the PSNR values demonstrate notable differences across different bpp settings. Our proposed method consistently exhibits higher PSNR values than the other methods, indicating superior image quality preservation. At 0.1 bpp, our proposed method achieved 40.522 dB, while Al Huti et al. [23], Syahlan and Ahmad [24] recorded 29.560 dB and 30.282 dB, respectively. This trend continued across various bpp settings, with our proposed method consistently outperforming in terms of PSNR for Baboon, as shown in Fig. 4(a).

Similarly, for the Peppers image, our proposed method showcased higher PSNR values across different bpp levels compared to Al Huti et al. [23], Syahlan and Ahmad [24]. At 0.1 bpp, our proposed method achieved 48.344 dB, surpassing Al Huti et al. [23], Syahlan and Ahmad [24], who recorded 38.112 dB and 36.685 dB, respectively. This trend persisted across different bpp settings, highlighting the enhanced visual quality preservation of our proposed method for the Peppers image, as shown in Fig. 4(b). For the medical images (Head, Leg, and X-Ray), a similar pattern emerged, as shown in Figs. 4(c), 4(d), and 4(e), indicating that our proposed method consistently provided better visual quality, as indicated by higher PSNR values across various bpp settings compared to the other methods (Al Huti et al. [23], Syahlan and Ahmad [24]). These results underscore the superiority of our proposed method in preserving image quality across different image types and bpp settings, making it a more favorable choice for reversible data embedding due to its superior visual quality retention.

4. Conclusion

Reversible data embedding techniques offer a promising solution by allowing the secure integration of additional data into digital images without compromising the original content. This method is particularly useful for sensitive images such as military, art, and medical images, where each pixel contains important information that requires authentication. In reversible watermarking, two crucial factors require enhancement: the resemblance between the cover image and the watermarked image, and the payload capacity. In this study, we developed a reversible watermarking method with block-based optimization based on Reduced Difference Expansion (RDE) applied to 3×3 pixel blocks, allowing for the embedding of $8-$bit data. Based on experimental results from tests conducted on two common images and three medical images, our method consistently achieved high payload capacity while maintaining good visual quality across various image categories, outperforming previous

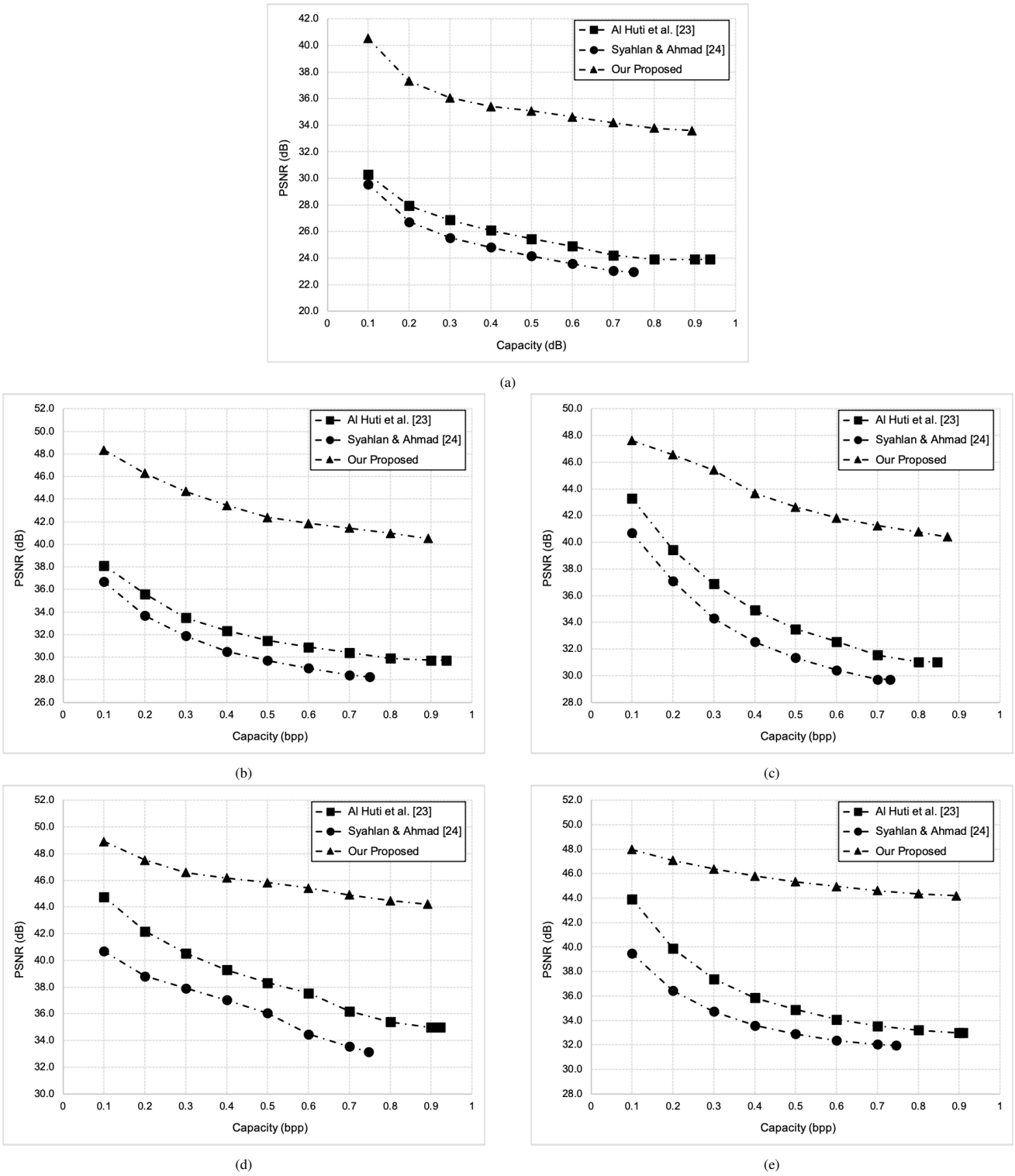

Fig. 4. Comparison between proposed method and the previously proposed method [23] and [24] in term of PSNR in different sizes of payload data (a) Baboon (b) Peppers (c) Head (d) Leg (e) X-Ray

approaches.

Acknowledgement

The authors gratefully acknowledge the support for the publication of this article provided by the Department of Electrical and Information Engineering, Faculty of Engineering, Universitas Gadjah Mada, through the Department Research Grant 2024.

References

1. W. Najib, S. Sulistyo, and Widyawan, *Tinjauan Ancaman dan Solusi Keamanan pada Teknologi Internet of Things*, J. Nas. Tek. Elektro dan Teknol. 9 (2020) 375-384.
2. T. P. Fiqar and T. Ahmad, *Peningkatan Kapasitas Penyisipan Audio Data Hiding Berbasiskan Modifikasi Metode Least Significant Digit*, J. Nas. Tek. Elektro dan Teknol. Inf. 6 (2017) 315–325.
3. I. Saputra, Y. Arkeman, I. Jaya, I. Hermadi, N. A. Akbar, and I. Sutedja, *AniraBlock: A leap towards dynamic smart contracts in agriculture using*

blockchain based key-value format framework, Commun. Sci. Technol. 8 (2023) 154–163.
4. C. R. Atmaja Perdana, H. Adi Nugroho, and I. Ardiyanto, *Comparison of text-image fusion models for high school diploma certificate classification*. Commun. Sci. Technol. 5 (2020) 5-9.
5. R. Anushiadevi and R. Amirtharajan, *Separable reversible data hiding in an encrypted image using the adjacency pixel difference histogram*. J. Inf. Secur. Appl. 72 (2023) 103407
6. S. Gull, N. A. Loan, S. A. Parah, J. A. Sheikh, and G. M. Bhat, *An efficient watermarking technique for tamper detection and localization of medical images*. J. Ambient Intell. Humaniz. Comput., 11 (2020) 1799–1808.
7. S. Kanwal, F. Tao, A. Almogren, A. Ur Rehman, R. Taj, and A. Radwan, *A Robust Data Hiding Reversible Technique for Improving the Security in e-Health Care System*. Comput. Model. Eng. Sci. 134 (2023) 201–219.
8. K. Nour and A. Al-Haj, *Reversible data hiding using bit flipping and histogram shifting*. Multimed. Tools Appl. 81(2022) 12441–12458.
9. V. M. Devineni, V. N. D. Pavuluri, and V. M. Manikandan, *A Detailed Review on Reversible Data Hiding and Its Applications. in International Conference on Soft Computing and Pattern Recognition, cham, 2023, pp. 413–423.*
10. A. Arham and N. Lestari, *Arnold's cat map secure multiple-layer reversible watermarking*. Indones. J. Electr. Eng. Comput. Sci. 33 (2024) 1536-1545.
11. A. Arham and N. Lestari, *Secure medical image watermarking based on reversible data hiding with Arnold's cat map*. Int. J. Adv. Intell. Informatics 9 (2023) 445-456.
12. A. Arham, H. A. Nugroho, and T. B. Adji, *Multiple Layer Data Hiding Scheme Based on Difference Expansion of Quad*. Signal Processing. 137 (2017) 52–62.
13. J. Tian, *Reversible data embedding using a difference expansion*. IEEE Trans. Circuits Syst. Video Technol. 13 (2003) 890–896.
14. J. Tian, *Wavelet-based reversible watermarking for authentication. in Security and Watermarking of Multimedia Contents IV, San Jose, California, United States, 2002, pp. 679–690.*
15. C.-L. Liu, D.-C. Lou, and C.-C. Lee, *Reversible Data Embedding Using Reduced Difference Expansion. in Third International Conference on Intelligent Information Hiding and Multimedia Signal Processing, 2007, pp. 433–436.*
16. H. Yi, S. Wei, and H. Jianjun, *Improved reduced difference expansion based reversible data hiding scheme for digital images," in International Conference on Electronic Measurement & Instruments, 2009, pp. 4–318.*
17. S. M. Abdullah and A. A. Manaf, *Multiple Layer Reversible Images Watermarking Using Enhancement of Difference Expansion Techniques," in Networked Digital Technologies: Second International Conference, NDT 2010, Prague, Czech Republic, July 7-9, 2010. pp. 333–342*
18. P. Maniriho and T. Ahmad, *Information hiding scheme for digital images using difference expansion and modulus function*. J. King Saud Univ. Inf. Sci. 31 (2019) 335–347.
19. A. M. Alattar, *Reversible watermark using difference expansion of triplets. in IEEE International Conference on Image Processing, ICIP'2003', 2003, pp. I-501–4.*
20. A. M. Alattar, *Reversible watermark using difference expansion of quads. in IEEE International Conference on Acoustics, Speech, and Signal Processing, 2004, pp. iii-377–80.*
21. J.-Y. Hsiao, K.-F. Chan, and J. M. Chang, *Block-based reversible data embedding*. Signal Processing 89(2009) 556–569.
22. T. Ahmad, M. Holil, W. Wibisono, and I. Royyana Muslim, *An improved Quad and RDE-based medical data hiding method. in Proceeding - IEEE CYBERNETICSCOM 2013: IEEE International Conference on Computational Intelligence and Cybernetics, 2013, pp. 141–145.*
23. M. H. A. Al Huti, T. Ahmad, and S. Djanali, *Increasing the capacity of the secret data using DEpixels blocks and adjusted RDE-based on grayscale images. in International Conference on Information & Communication Technology and Systems, 2015, pp. 225–230.*
24. Z. Syahlan and T. Ahmad, *Reversible data hiding method by extending reduced difference expansion*. Int. J. Adv. Intell. Informatics. 5 (2019) 101–112.
25. I.-C. Dragoi and D. Coltuc, *Local-Prediction-Based Difference Expansion Reversible Watermarking*. Image Processing, IEEE Transactions on. 23 (2014) 1779–1790.
26. P. C. Mandal, I. Mukherjee, and B. N. Chatterji, *High capacity reversible and secured data hiding in images using interpolation and difference expansion technique*. Multimed. Tools Appl. 80 (2021) 3623–3644.
27. Y. Chen, W. Sun, L. Li, C.-C. Chang, and X. Wang, *An efficient general data hiding scheme based on image interpolation*. J. Inf. Secur. Appl. 54 (2020) 102584.
28. X. Bai, Y. Chen, G. Duan, C. Feng, and W. Zhang, *A data hiding scheme based on the difference of image interpolation algorithms*. J. Inf. Secur. Appl. 65 (2022) 103068.
29. F. S. Hassan and A. Gutub, *Novel embedding secrecy within images utilizing an improved interpolation-based reversible data hiding scheme*. J. King Saud Univ. - Comput. Inf. Sci. 34 (2022) 2017–2030.
30. M. S. Hossen, T. Ahmad, and N. J. D. L. Croix, *Data Hiding Scheme using Difference Expansion and Modulus Function, in 2023 2nd International Conference for Innovation in Technology (INOCON), 2023, pp. 1–6.*
31. T.-C. Lu, *Interpolation-based hiding scheme using the modulus function and re-encoding strategy*. Signal Processing 142 (2018) 244–259.
32. A. Laffont, P. Maniriho, A. Ramsi, G. Guerteau, and T. Ahmad, *Enhanced pixel value modification based on modulus function for RGB image steganography," in 2017 11th International Conference on Information & Communication Technology and System (ICTS), 2017, pp. 61–66.*
33. W. He and Z. Cai, *Reversible Data Hiding Based on Dual Pairwise Prediction-Error Expansion*. IEEE Trans. Image Process. 30 (2021) 5045–5055.
34. W. He and Z. Cai, *An Insight Into Pixel Value Ordering Prediction-Based Prediction-Error Expansion*. IEEE Trans. Inf. Forensics Secur. 15 (2020) 3859–3871.
35. I.-H. Pan, P.-S. Huang, T.-J. Chang, and H.-H. Chen, *Multilayer Reversible Information Hiding with Prediction-Error Expansion and Dynamic Threshold Analysis*. Sensors 22, (2022) 4872.
36. T.-C. Lu, C.-C. Chang, and Y.-H. Huang, *High capacity reversible hiding scheme based on interpolation, difference expansion, and histogram shifting*. Multimed. Tools Appl. 72 (2014) 417–435.
37. Y. Jia, Z. Yin, X. Zhang, and Y. Luo, *Reversible data hiding based on reducing invalid shifting of pixels in histogram shifting*. Signal Processing 163 (2019) 238–246.
38. A. Mehbodniya, B.K. Douraki, J.L. Webber, H.A. Alkhazaleh, E. Elbasi, M. Dameshghi, R. Abu Zitar, and L. Abualigah, *Multilayer Reversible Data Hiding Based on the Difference Expansion Method Using Multilevel Thresholding of Host Images Based on the Slime Mould Algorithm*. Processes 10 (2022) 858.